Plate Deformation in the Welding Process of Three Plates

Huynh Nguyen Hoang [1], Pham Son Minh [*2]
HCMC University of Technology and Education, Ho Chi Minh City, Vietnam

Abstract

This study focuses on the welding deformation via simulation and experiments. The structure of a combined joint geometry was modeled and simulated using the Simufact welding software based on the thermo-elastic-plastic approach. To verify the simulation results, a series of experiments was conducted with three plates of low carbon steel AISI 1005 as the parent metal and digital gas metal arc welding (GMAW) power source with premixed shielding gas and the one-sided clamping technique. It was established that the results of the thermo-elastic-plastic 3D FEM analysis show good agreement with the experimental results, and the welding process 7 induced less distortion compared with other processes. By assuming the location of one plate, the deformation almost finds the location of the other free plates.

Keywords—*Welding simulation, structure deformation, heat transfer, plate connection, plate distortion.*

I. INTRODUCTION

In the arc welding field, the welding parameters are often selected by standards such as API and ASME. These standards ensure the strength of the welding connection [1]. In the arc welding process, the structure will be locally heated. This causes thermal stress and significant part distortion occurs, especially at the weld area [2]. This deformation is a serious problem for the structure, especially for the assembly part. For solving this problem, the experiment of the designer is an important element. However, the experiment is just useful with the common product geometry. With the new product, predicting the part deformation in the welding process is a big issue.

In recent years, structural deformation can be simulated and observed using numerical method [1–4]. However, this makes it difficult to model the welding structure via the finite element method (FEM). Due to the intense concentration of heat in the heat source of welding, the regions near the weld line experience numerous boundary conditions such as clamping force, heat transfer, and heating source [3, 4]; hence, predicting 3D weld deformation is a major topic for welding engineering alloys.

In recent years, with the development of computer and software technologies, 3D simulation of welding can be achieved. Many researchers have studied thermal distributions and residual stresses in welding. Teng et al. [5] studied about the residual stresses during multi-pass arc welding in steel pipes using finite element (FE) techniques and discussed the effects of pipe diameter and wall thickness on weld residual stresses. Adaptive mesh refinements were used to transport the results between the different meshes [6]. The thermomechanical model and the simulation methodology that were used in this study are detailed. Computed distortions and residual stresses were compared with experimental measurements. Butt welding was simulated [7] for stainless steel pipes in a nonlinear thermomechanical FE analysis. In particular, the axial and hoop stresses and their sensitivity to variation in weld parameters were studied. In addition, numerous researchers performed a combined analytical and experimental method to analyze the residual stresses in a pipe formed with a girth-butt weld [4–8].

To simulate the single pass welding [9], the present investigation utilizes an element “birth” and “death” FE technique to step-by-step control the process of filling the metal during welding process. The dynamic thermal distributions and strain evolutions are simultaneously analyzed in a 10-mm plate-butt SUS310 stainless steel in the multi-pass welding using FEM. The comparison between the calculated driving force and material resistance predict the weld metal deformation.

This study aims to develop an efficient method to reduce the design time and improve the accuracy for welding structure manufacturing. Here, a model considering both material properties and welding zone situation is analyzed. The local inherent stress of the welding bead is represented by an equivalent moment and other parameters, and then, a novel welding simulation software is proposed to predict the welding deformation.

II. SIMULATION AND EXPERIMENT

Fig. 1 shows the simulation procedure for gas metal arc welding (GMAW). Based on this progression, the welding process will be designed according to the American Welding Society standards. Then, from the research model, the welding geometry will be created. All the welding models are meshed, and the boundary condition is set up. All the data will be used for the simulation running. Then, the software shows the result of temperature distribution,

deformation, and the residual stress of all welding structures. Fig. 2 shows that the double ellipsoid heat source model is applied to the base metal as the heat source model [8, 9]. In this study, the parameters of Goldak's model are used, shown in Table 1.

Fig. 3 shows the mesh of the welded plate under investigation. In the 3D solid model established using the simulation software Simufact, 43,855 elements are used. Fine mesh is used around the weld, whereas coarse mesh is used away from the weld. The meshes of welding passes are ignored because a single layer is used in this study. A low-alloy high-tensile steel was adopted herein. Its carbon content varied from 0.14% to 0.22%. The other chemical properties are shown in Table 2. Table 3 shows the material properties of the welding plate. At the situation of ambient temperature, Poisson's ratio is 0.33, density is 7.8 kg/m^3, and melting point is 1404 ◦C [6]. In the heat analysis near the weld molten pool zone, mainly heat radiation appears. However, the farther place mainly appears surface heat exchange.

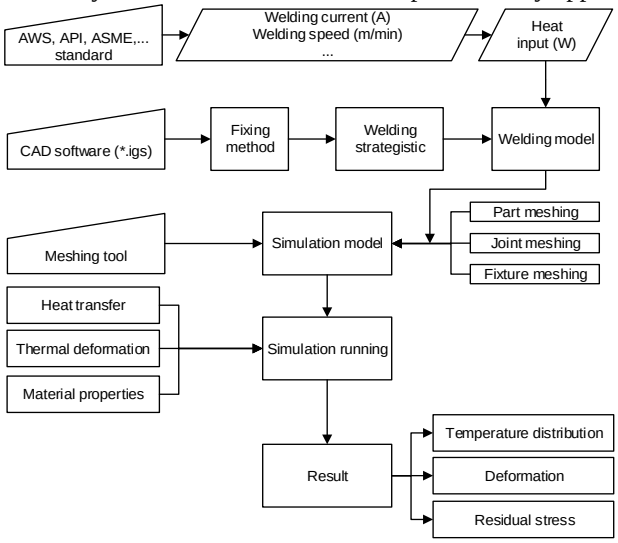

Fig. 1 Simulation Procedure.

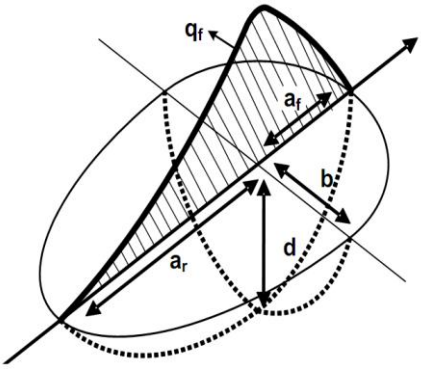

Fig. 2 Goldak's Model.

Table I : Parameters of Goldak's Double Model

Parameters of Goldak's double ellipsoid	
a_f	4 mm
a_r	7 mm
b	3.5 mm
d	3 mm

Table II : Chemical Low Carbon Steel

Standard	AISI 1005
% C	0.14–0.22
% Si	0.12–0.30
% Mn	0.40–0.65

TABLE III : Material Properties of Welding Plates [7]

Material properties	
Young's Modulus at 20 °C	210 GPa
Minimum yield strength	355 MPa
Poisson's ratio	0.33
Solidus temperature	1404 °C
Liquidus temperature	1505 °C

Fig. 4 shows the welding model with the original coordinate. The Y-axis is the plate width direction, the X-axis is the welding direction, and the Z-axis is the plate thickness direction. The units in weld zone are activated one by one during the welding process. The welding processes are shown in Fig. 5.

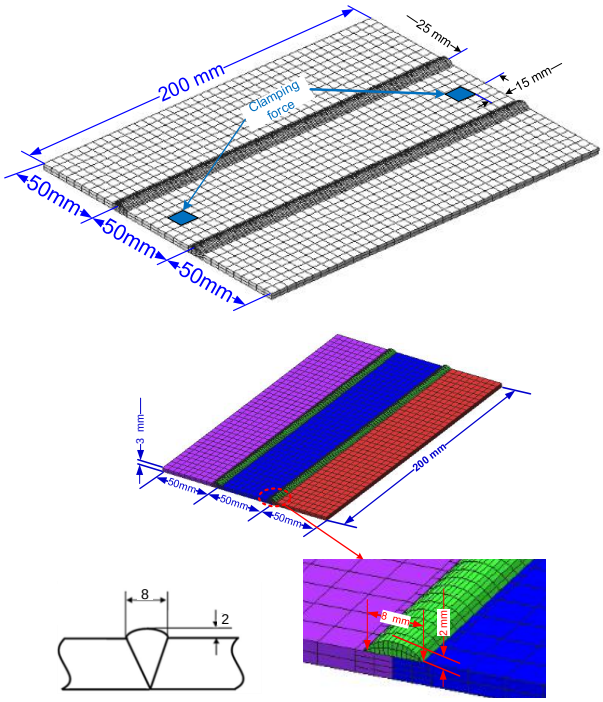

Fig. 3 Mesh Model for Simulation.

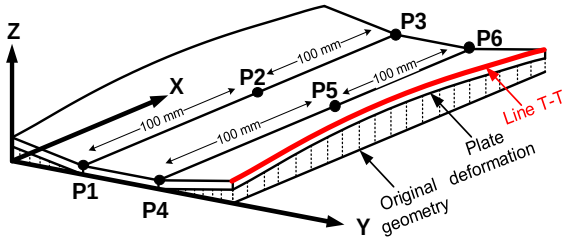

Fig. 4 Location for Observing the Welding Deformation.

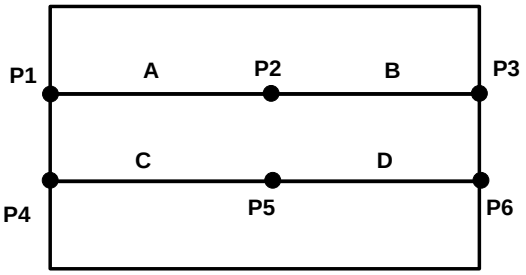

A+: From P1 to P2. C +: From P4 to P5.
A −: From P2 to P1. C −: From P5 to P4.
B +: From P2 to P3. D +: From P5 to P6.
B −: From P3 to P2. D −: From P6 to P5.

Fig. 5 Welding Processes.

Table IV : Welding Processes

Process No	Welding schedule			
	A	B	C	D
1	–	–	–	–
2	+	–	–	–
3	–	+	–	–
4	+	+	–	–
5	–	–	+	–
6	+	–	+	–
7	–	+	+	–
8	+	+	+	–
9	–	–	–	+
10	+	–	–	+
11	–	+	–	+
12	+	+	–	+
13	–	–	+	+
14	+	–	+	+
15	–	+	+	+
16	+	+	+	+

TABLE V : Welding Parameters Used for Simulation and Experimental Method

Welding parameter	Value
Current	90 A
Voltage	21.6 V
Welding speed	5.7 mm/s

In this study, a linear elastic shrinkage method with a relatively new FEM software, Simufact Welding, developed by Simufact Engineering GmbH, is employed to simulate the welding process and to predict the welding distortion in a 3-mm-thick butt joint. For verification, a series of experiments were performed using a fully automated welding system with a GMAW power source. The shielding gas for the welding process was carbon dioxide (CO_2). To measure the initial and final dimensions of the specimen, a coordinate measuring machine was used. The welding parameters used during the experiments are shown in Table 5. For observing the influence of the welding process on the deformation of a structure, 16 processes were designed for simulation and experiment. The description of the welding process is shown in Fig. 5 and Table 4.

III.RESULTS AND DISCUSSIONS

The deformation of the plates at the end of the welding cycle is shown in Fig. 6 and 7. In the different processes, as shown in Table 4, the deformation of the three plates is almost the same with different processes. The fixed plate has smaller deformation than the other plates. The maximum deformation is located at line T–T (Fig. 4) because the clamping fore position and deformation of the plate are strongly limited. Therefore, in the welding cycle, the thermal deformation clearly decreased. On the contrary, the free plate was warped by the thermal stress. Since the weld only appears at the top surface, the stress distribution on the top surface is greater than that on the bottom surface because of the thermal imbalance of the two sides [14, 15].

By comparing the deformation values among the 16 processes, we found that maximum deformation was observed for process 1, which has the distortion ranging from −5.56 mm to 6.04 mm, and the value was lower for the other processes. The reduction could be explained by thermal stress. In process 1, the thermal energy appeared at the welding line from point 1 to point 3. That is, with the same welding time, the plates in process 1 continuously received thermal energy, and consequently, the heat concentrate appeared more clearly at the welding position. Hence, the thermal stress for process 1 is greater than that for the other processes. In processes 2 and 3, although the welding time is the same as that for process 1, the welding cycle includes two steps. Therefore, the heat concentration clearly reduced and the residual stress decreased.

The plate deformation on line T–T is also studied. The results were collected and compared in Fig. 8. It is clear that processes 2 and 3 have greatly improved plate deformation. In addition, the deformation distribution on line T–T shows that maximum distortion points are affected by the welding process.

In process 1, when the plates were continuously welded from point 1 to point 3, the larger deformation is located at the side of point 3. This result could be explained by thermal deformation. At the beginning of the welding cycle, both plates were cooled. Therefore, thermal deformation did not occur. However, when the welding process started, the plates were heated, and thermal deformation occurred. The longer the welding time, the more the deformation. The temperature distribution can clearly be observed in Fig. 6c. By simulation, the maximum distortion occurred at point 110.5 mm on X-axis.

In general, process 7 shows the best result of deformation. By comparing the deformation distribution, the maximum distortion in process 7 is 2.60 mm and is located at the center (X = 112.4 mm) and to the right (X = 162.0 mm). The location of maximum deformation can be explained by the temperature distribution as well as the residual stress. In process 7, the highest temperature is located between point 2 and 3 (Fig. 6). This difference in maximum temperature leads to the change in the residual stress.

Process 1

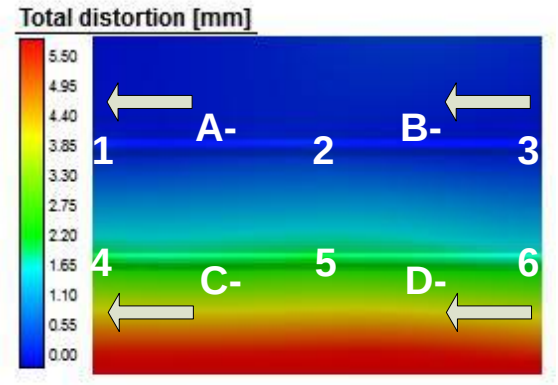

Min: 0.12 Max: 6.25

Process 2

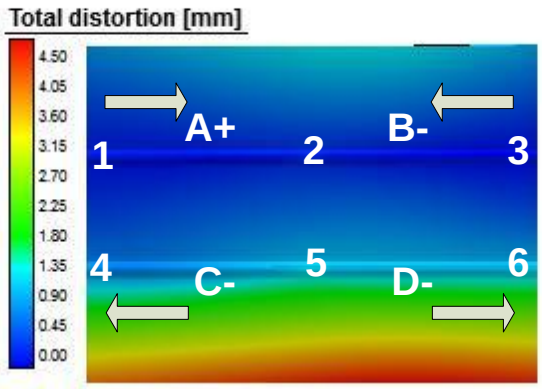

Min: 0.01 Max: 4.47

Process 3

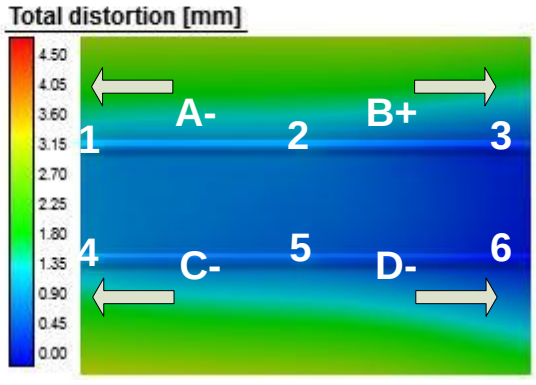

Min: 0.07 Max: 3.04

Process 4

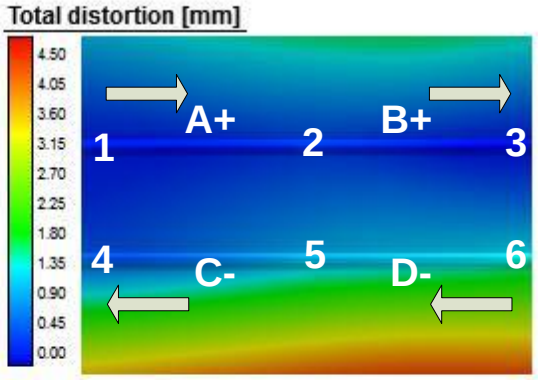

M

in: 0.02 Max: 4.14

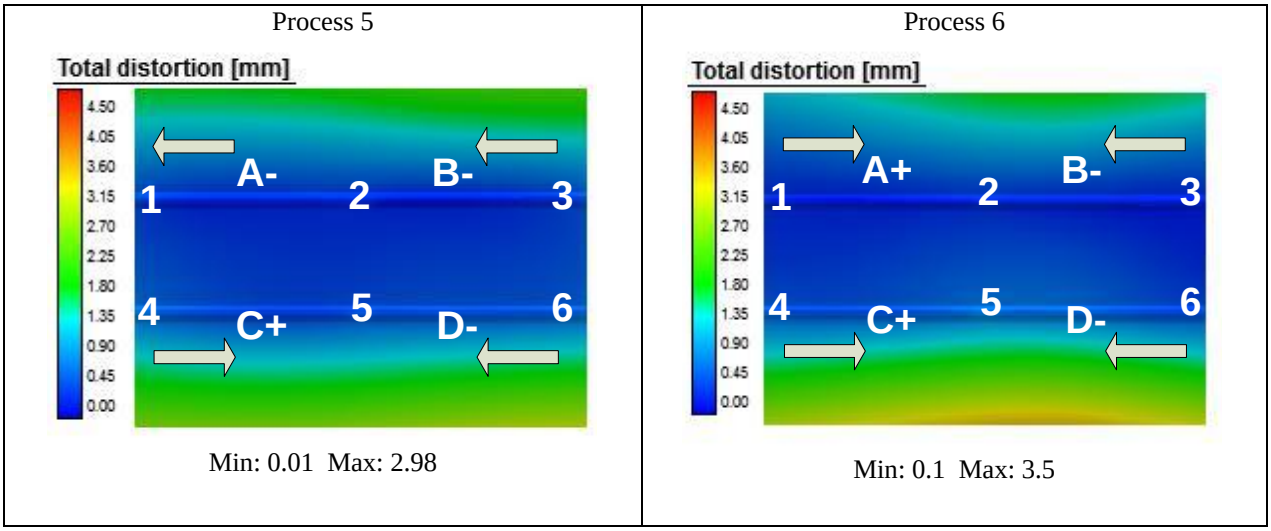

Fig. 6 Simulation Results at the End of the Welding Cycle For Processes 1–6.

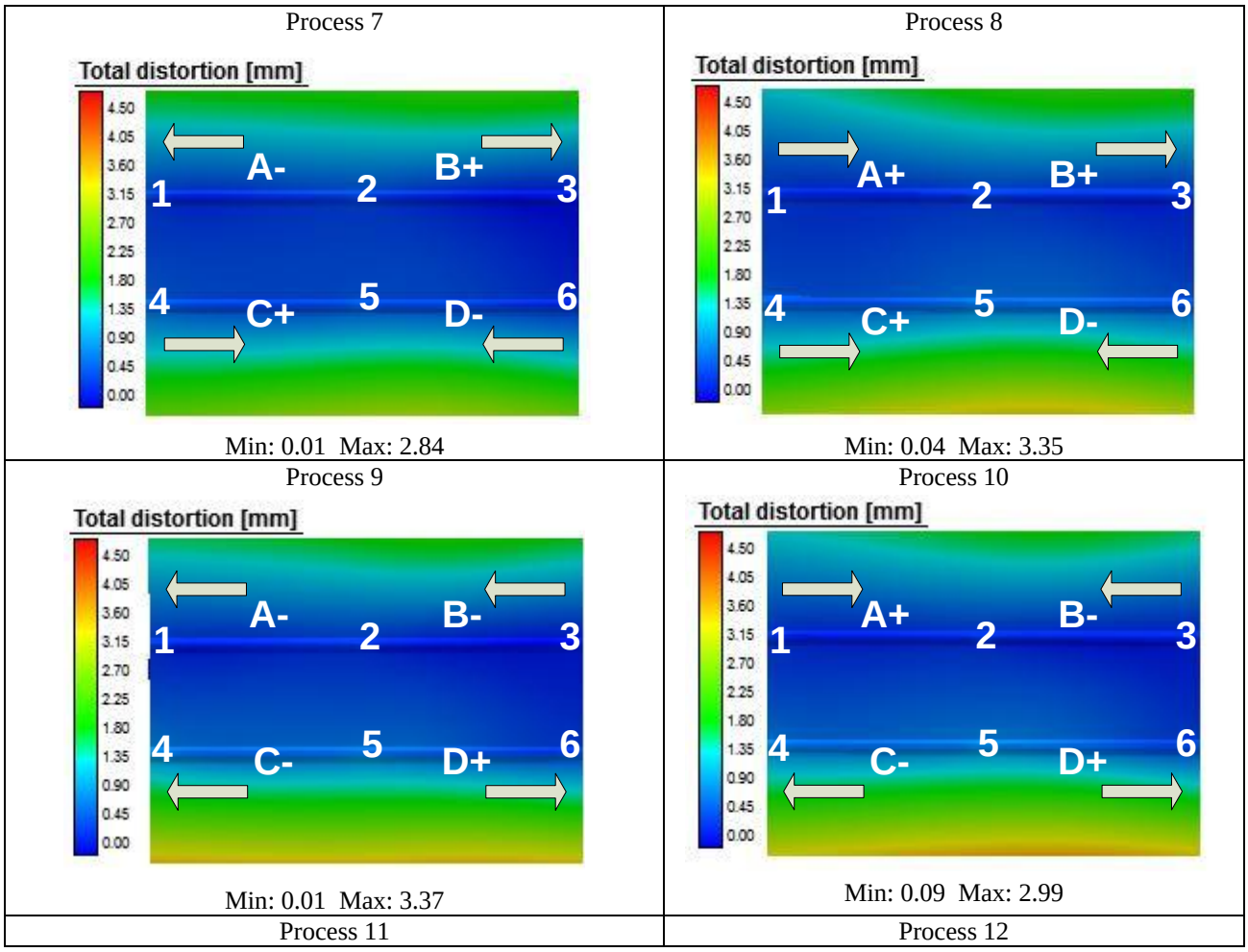

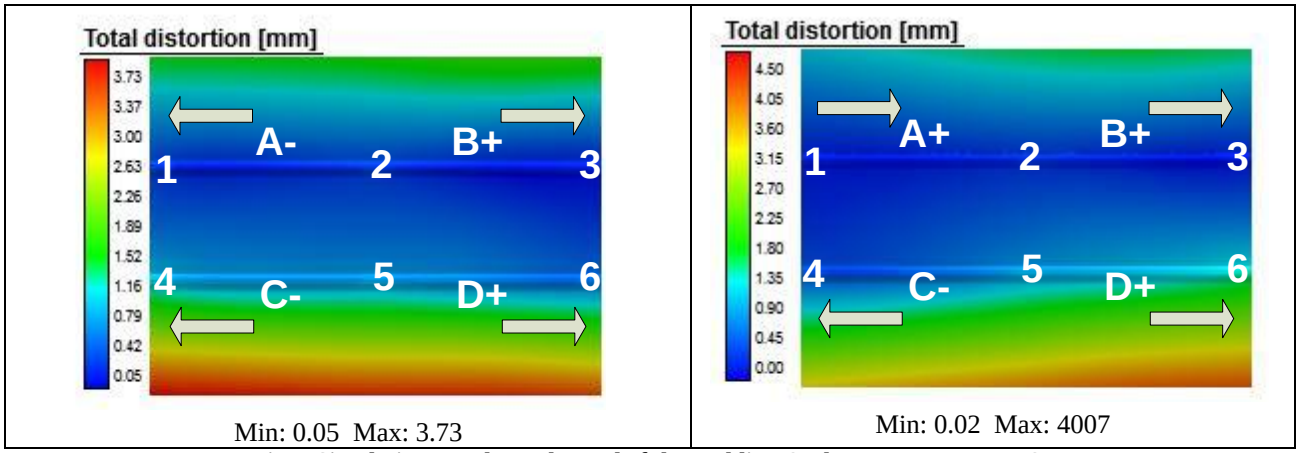

Fig. 7 Simulation Results at the End of the Welding Cycle For Processes 7–12.

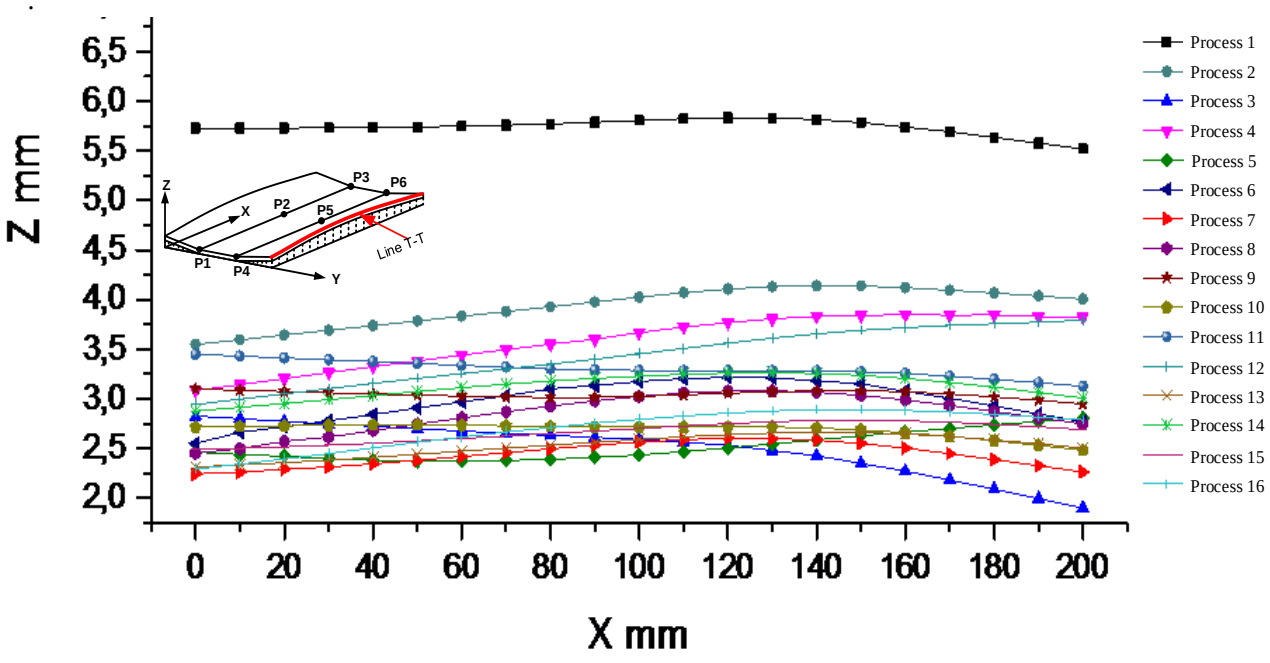

Fig. 8 Simulation Result of Plate Deformation on Line T–T.

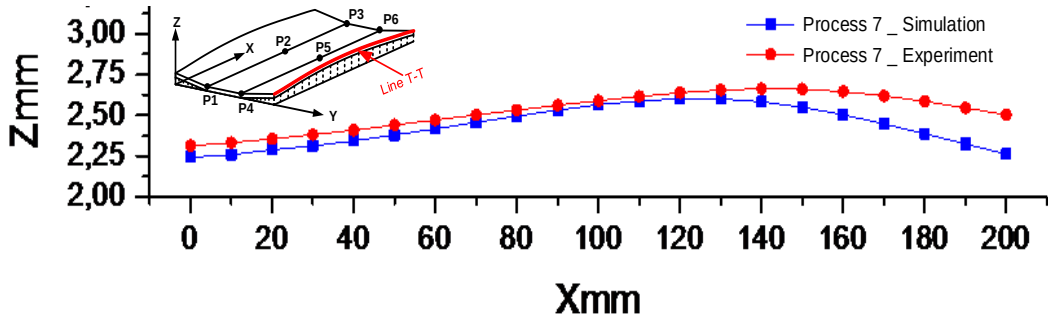

Fig. 9 Plate Deformation on Line T–T with Different Processes

To verify the simulation accuracy, the GMAW processes were experimentally observed. Each process was performed 10 times. Then, the average deformation on line T–T was measured and compared with the simulation result. The experiment results are shown in Fig. 9. The simulation and experiment results show good agreement. The difference between simulation and experiment occurs at the end of line T–T (X = 200 mm) because of the effect of the heat transfer coefficient and the heat conductivity of the plate's material. In the simulation, these properties were given ideal values. However, in the experiment, these parameters cannot be exactly the same as those used in the simulation. In the experiment, since heat

transfer is not as fast as the ideal material, at the end of welding cycle, the temperature of the real plate is higher than that of the simulated plate. This is the main reason for the different deformations between the simulation and experiment.

IV. CONCLUSIONS

In this study, GMAW was performed on three metal plates. Three types of GMAW were established. The plate deformation for different processes was observed and compared. Based on these results, the following conclusions are obtained:

- By assuming the location of one plate, the deformation almost finds the location of the other free plates.

- In the 16 processes, the deformation profiles are almost the same. However, the deformation values considerably change. The biggest deformation appears for process 1 and reduces strongly for the other processes.

- The simulation can accurately predict the deformation.

REFERENCES

[1] H. Bergmann, and R. Hilbinger, "Numerical simulation of centre line hot cracks in laser beam welding of aluminum close to the sheet edge," International seminar; 4th, Numerical analysis of weld ability, Institute of material, pp. 658–668, 1998.

[2] Z. L. Feng, and C. L. Tsai, "A computational analysis of thermal and mechanical conditions for weld metal solidification cracking," Welding in the World, vol. 33 (5), pp. 340–347. 1994.

[3] C. D. Elcoate, R. J. Dennis, and P. J. Bouchard, "Three dimensional multi-pass repair weld simulation," International Journal of Pressure Vessels and Piping, vol. 82 (4), pp. 244–257, April 2005.

[4] Z. B. Dong, and Y. H. Wei, "Three dimensional modeling weld solidification cracks in multipass welding," Theoretical and Applied Fracture Mechanics, vol. 46 (2), pp. 56–165, Oct. 2006.

[5] T. J. Teng, and P. H. Chang, "A study of residual stresses in multi-pass girth-butt welded pipes," International Journal of Pressure Vessels and Piping, vol. 74 (1). Pp. 59–70, Nov. 1997.

[6] P. Duranton, J. Devaus, J., and V. Robin, "3D modelling of multipass welding of a 316L stainless steel pipe," Journal of Materials Processing Technology, vol. 153–154, pp. 457–463. Nov. 2004.

[7] B. Brickstad, and B. L. Josefson, "A parametric study of residual stresses in multi-pass butt-welded stainless steel pipes," International Journal of Pressure Vessels and Piping, vol. 75 (1), pp. 11–25. Jan. 1998.

[8] P. J. Bouchard, and D. George, "Measurement of the residual stresses in a stainless steel pipe girth weld containing long and short repairs," International Journal of Pressure Vessels and Piping, vol. 105 (4), pp. 81–91. Apr. 2005.

[9] J. R. Cho, B. Y. Lee, and Y. H. Moon, "Investigation of residual stress and post weld heat treatment of multi-pass welds by finite element method and experiments," Journal of Materials Processing Technology, vol. 155–156, pp. 1690–1695. Nov. 2004